Comparison of Experimental and Computational Fluid Dynamics Studies of Slug Flow in a Vertical 90 ^{o} Bend

M. Abdulkadir, V. Hernandez-Perez, S. Lo, I. S. Lowndes and B. J. Azzopardi

Reprinted from

The Journal of
Computational Multiphase Flows

Volume 5 · Number 4 · 2013

Multi-Science Publishing

Comparison of Experimental and Computational Fluid Dynamics (CFD) Studies of Slug Flow in a Vertical 90º Bend

Abdulkadir, M.[1, 2, 3*], Hernandez-Perez, V.[1], Lo, S.[4], Lowndes, I. S.[1] and Azzopardi, B. J.[1]
[1]Process and Environmental Engineering Research Division, Faculty of Engineering, University of Nottingham University Park, Nottingham, NG7 2RD, United Kingdom
[2]Department of Chemical Engineering, Federal University of Technology, Minna, Niger State, Nigeria
[3]Department of Petroleum Engineering, African University of Science and Technology (AUST), Abuja, Nigeria
[4]CD-adapco, Trident Park, Didcot, OX11 7HJ, United Kingdom

Received: 6 August 2013, Accepted: 20 December 2013

Abstract
This paper presents the results of comparison of experimental and CFD studies of slug flow in a vertical 90º bend using validated models. For the experimental part, Electrical Capacitance Tomography (ECT), Wire Mesh Tomography (WMS), and high-speed videos were used to monitor an air-silicone oil mixture flowing in a vertical 90o bend. The ECT probes were mounted before the bend whilst the WMS was positioned either immediately upstream or immediately downstream of the bend. The downstream pipe was maintained horizontal whilst the upstream pipe was maintained vertical. The bend (R/D = 2.3) was made of transparent acrylic resin. Parallel to the experiments, simulations were carried out for same experiment set-up using the commercial software package Star-CD and Star-CCM+. The condition was simulated with the Volume of Fluid (VOF) model. The simulation predictions were validated against the experimental data. A reasonably good agreement was observed for the results of the experiment and CFD.

Key words: CFD, ECT, VOF, Slug flow, air-silicone oil

1. INTRODUCTION

Slug flow is one of the most common flow patterns in two-phase flow and is one of the most frequently occurring flow situations in many problem areas of practical importance (Bagci [8]). In the oil and gas industry, two-phase flow is encountered during the production and transportation of oil and gas. The flow occurs in both wellbores and flow lines and involves horizontal, inclined and vertical pipes. A common scenario when there is a change in flow direction from vertical to horizontal, here the fitting can be considered as a control volume that consists of three different sections: vertical pipe, horizontal pipe and bend section. Slug flow through separate pipelines, whatever the inclination is, is relatively well understood; however, there is a lack of understanding on how flow characteristics are changed when these pipe sections are joined into one by a bend. One feature of slug flow is the acceleration of the liquid phase to form fast moving liquid slugs, which can carry a significant amount of liquid with high kinetic energy. This is potentially hazardous to the structure of the flow transport system and processing equipment due to the strong oscillating pressure produced by the mechanical momentum of the slugs Abdulkadir [1]. This can pose challenges to the design and operation of such flow systems.

A considerable amount of research has been devoted to the study of this two-phase flow regime. Examples of such research workers are: Akagawa and Sakaguchi [7], Barnea and Brauner [9], [11-12], [14-15], [17-18], [20], [30-32], [34], [36], [38], [41], and [43-44] among others. A critical

*Corresponding author s e-mail: mukhau@futminna.edu.ng

review of this topic is given by Fabre and Line [19]. However, there remains much to be investigated and understand about that flow pattern. Moreover, reports on slug flow behaviour with fluids which are relevant to the industry are limited. Empirical correlations and mechanistic models have been presented in the literature. These are mainly one-dimensional approaches that cannot fully characterize the flow. The limitations of one-dimensional models may be addressed by the use of Computational Fluid Dynamics (CFD). The applications of CFD to investigate multiphase flow are highly dependent on the flow pattern under study, as different closure models are needed for different flow regimes. These models require to be validated to gain confidence in their use. The validation of CFD models requires experimental data that characterize the important flow parameters and over a wide range of values.

This work therefore aims to compare the results obtained from CFD simulation and experiment both before and after the vertical 90º bend based on time series of void fraction, probability density function (PDF) of void fraction and cross-sectional contour plot of void fraction.

2. EXPERIMENTAL ARRANGEMENT

The experimental investigations were carried out on an inclinable pipe flow rig within the Chemical Engineering Laboratories of University of Nottingham. The details of the experimental facility can be found elsewhere, (e.g. Abdulkadir *et al.* [2-3], [5], and [21-23]). In brief: the experimental test section of the facility consists of a transparent acrylic pipe of 6 m length and 0.067 m internal diameter. The test pipe section may be rotated on the rig to allow it to lie at any inclination angle of between -5 to 90º to the horizontal. For the experiments reported in this paper the rig test pipe section was mounted as a vertical riser (an inclination of 90º to the horizontal). It is worthy of mention that full-experimentation in risers attached to vertical 90º bends of this magnitude, and other larger ones, is expensive. Therefore a more cost-effective approach for exploring the behaviour of two-phase flow around these bends is by using validated CFD codes.

The resultant flow patterns created for the range of air–oil injection flow rates studied were recorded using electrical capacitance tomography (ECT) and wire mesh sensor (WMS). A detailed description of theory behind the ECT technology can be found elsewhere, for example, Azzopardi *et al.* [6], [25], [27], and [46]. In this study, a ring of electrodes were placed around the circumference of the riser at a given height above the injection portals at the bottom of the 6 m riser section. This enabled the measurement of the instantaneous distribution of the flow phases over the cross-section of the pipe. The use of two of such circumferential rings of sensor electrodes, located at a specified distance apart (also known as twin-plane sensors), enabled the determination of the rise velocity of any observed Taylor bubbles and liquid slugs. For details of the characterization of slug flow in a riser using both experiments and CFD, the reader is referred to [1]. The twin-plane ECT sensors were placed at a distance of 4.4 and 4.489 m upstream of the air–silicone oil mixer injection portal located at the base of the riser.

The capacitance WMS technology, placed at 4.92 m away from the mixing section, described in detail by da Silva *et al.* [16], can image the dielectric components in the pipe flow phases by measuring rapidly and continually the capacitances of the passing flow across several crossing points in the mesh. It consists of two planes of 24 stainless steel wires with 0.12 mm diameter, with a 2.78 mm wire separation within each plane and 2 mm axial plane displacement. This determined the spatio/temporal resolution of the sensor. Since the square sensor is installed in a circular tube, only 440 of the total 576 wire crossing points are within the radius of the tube [2]. During the experiments, the transmitter lines are pulsed one after another. By measuring the signal of all crossing orthogonal receiver wires, the local capacitance at the crossing points in the mesh is determined. This capacitance signal is a measure for the amount of silicone oil, and thus indicates the local phase composition in the grid cell.

Parallel to the experiments, CFD calculations were carried out. The aim of the numerical simulations is the validation of prediction of the slug flow with the existing multiphase flow models, built in the commercial code Star-CD and Star-CCM+.

3. NUMERICAL MODEL IMPLEMENTATION

This work is a follow up of the work presented previously by [1]. Here, a vertical 90º bend is attached to the vertical riser used in Abdulkadir *et al.* [4]. For details about the riser; the reader is referred to [4]. The motion of the Taylor bubbles rising in a flowing liquid through a vertical 90º

bend attached to a 67 mm internal diameter and 6 m height riser has been simulated using the commercial CFD tools Star-CD, as a pre-processor, and Star-CCM+ as the processor and post-processor. The numerical model implementation is similar to that used in [1] and [24], and here a summary is given for the sake of completeness, taken from the previous references.

3.1 Computational Domain

In order for the simulation to produce meaningful results, it was important to ensure that the geometry of the flow domain represented that of the experimental arrangement [3]. In view of this, a full 3-Dimensional domain, as shown in Figure 1, was considered. In this work, three CFD monitoring sections were placed before the bend at positions similar to those of the experimental work, namely, 4.4 m, 4.489 m and 4.92 m. Here, the locations 4.4 m and 4.489 m represent the two electrical capacitance tomography (ECT) planes whilst 4.92 m, the wire mesh sensor (WMS). For after the bend, one measurement section using the WMS was placed at a position similar to the experiment, 0.21 m downstream of the bend. Air and silicone oil are supplied at the inlet section of the pipe, then the two-phase mixture flowed along the vertical riser followed by the bend, and finally the two-phase flow is discharged through the outlet at atmospheric pressure. The relevant fluids properties are shown in Table 1.

Table 1: Properties of the fluids

Fluid	Density(kg/m^3)	Viscosity(kg/ms)	Surface tension (N/m)
Air	1.18	0.000018	
Silicone oil	900	0.0053	0.02

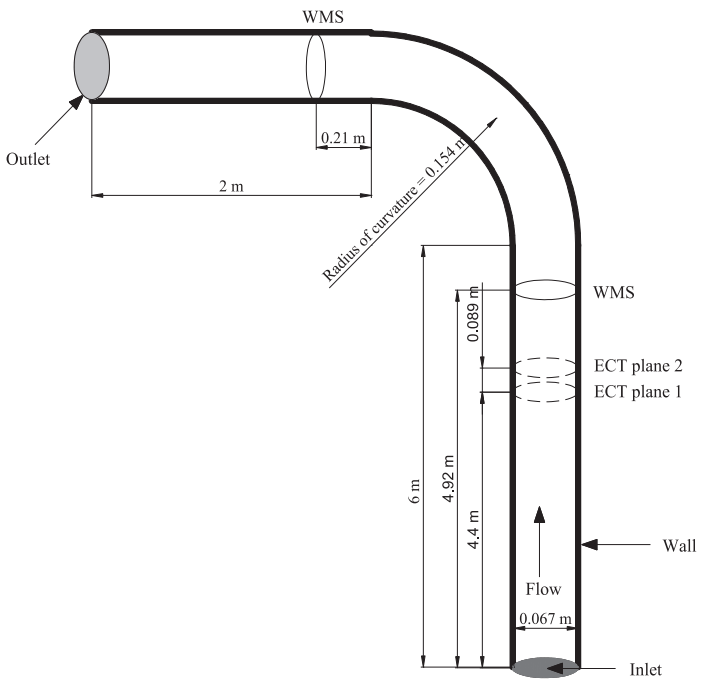

Figure 1: 3-D geometry of the computational domain showing the measurement locations and instrumentation.

3.2 Grid Generation

It has been reported by Hernandez-Perez *et al*. [24] and confirmed by [1] that the mesh has a great influence on the solver convergence and solution of every CFD simulation, as it is important to adopt high quality mesh standards to ensure the convergence and accuracy of the numerical simulation. The model geometry was built and meshed with Star-CD, then imported into Star-CCM+, where the computation and post-processing of the results were performed. The type of the mesh employed is the butterfly grid (O-grid), which has been successfully employed by [1], [23-24], and [29]. In this grid, a Cartesian mesh is used in the centre of the pipe combined with a cylindrical one around it. It requires multiple blocks but generally has the best grid quality in terms of orthogonality and mesh density. The construction of this mesh requires a more elaborated procedure, but it can be automated by implementing a macro in the Star-CD software. Details can be found in [1], [24], or [39]. The mesh density was selected based on the grid convergence study carried out in [1] and [39], where a mesh with 500,000 cells in a vertical 90° bend attached to vertical pipe of 6 m length and 67 mm diameter was found to be adequate for an inlet flow condition that consists of liquid and gas superficial velocities of 0.05 m/s and 0.34 m/s, respectively.

In brief: the mesh sensitivity study is performed with a constant ratio $\frac{\Delta t}{\Delta x} = 1\times10^{-4}$ and the mesh sizes of 350,000, 500,000, and 600,000 cells. The information about the meshes is shown in Table 2.

Table 2: Details of computational meshes

Mesh	Number of cells	Number of cells in cross-section	Number of rows in axial direction
Mesh 1	350,000	1750	200
Mesh 2	500,000	2500	200
Mesh 3	600,000	3000	200

The mesh sensitivity analysis revealed that the simulation with Mesh 1 under predicted the void fraction by 20 % based on the L^2 error method. The L^2 error was determined using equation 1.

$$L^2 = \frac{\sum (Y_{measured} - Y_{simulated})^2}{\sum Y^2_{measured}} \tag{1}$$

Where Y is the time average of the variable for which the error is computed
The purpose of this is to compare the predictions once the code has reached a steady-state.

The L^2 error between the measured and simulated void fraction was reduced to 5 % by applying Mesh 2. The comparison between the results obtained from Mesh 2 and Mesh 3 indicate that the results do not significantly depend on further mesh improvement. Details can be found in [1]. Figure 2 shows the selected mesh (Mesh 2).

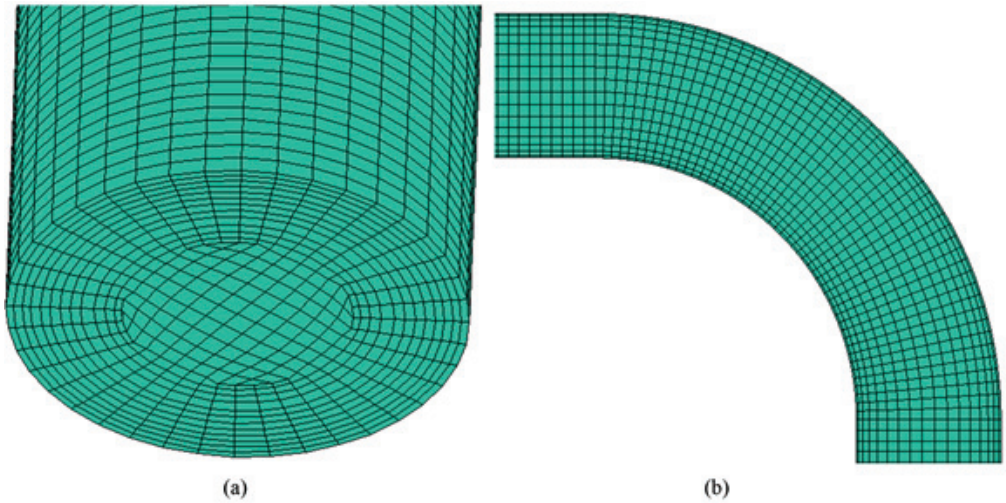

Figure 2: Computational mesh used for simulation

3.3 Governing equations

The movement of an incompressible gas–liquid two-phase slug flow under isothermal conditions has been considered as the flow scenario in the present work. According to [1], the assumption of an isothermal flow is a reasonable approximation for pipes which have a large surface area to volume ratio and a constant temperature. The Volume of Fluid (VOF) method, based on the Eulerian approach, implemented in the commercial CFD package Star-CCM+ is used in the numerical simulation. In addition, Star-CCM+ [37] use a High Resolution Interface Capturing Scheme (HRIC) based on the Compressive Interface Capturing Scheme for Arbitrary Meshes (CISCAM) introduced by Ubbink [40] and enhanced by [33]. In the VOF method, the fields for all variables and properties are shared by the phases and represent volume-averaged values, as long as the volume fraction of each of the phases is known at each location.

The resulting set of governing equations for the two-phase flow through the domain include: mass, momentum and volume fraction conservation equations, represented as equations (2), (3) and (5), respectively:

The continuity equation ensures mass balance is maintained in the system.

$$\frac{\partial \rho}{\partial t}+\frac{\partial \rho u_i}{\partial x_i}=0 \tag{2}$$

The momentum equation, equation (3), is dependent on the volume fractions of all phases through the properties ρ and μ. The body forces in the momentum equation consist of gravitational and surface tension forces. Surface tension along an interface arises as a result of attractive forces between molecules in a fluid. The continuum surface force (CSF) model proposed by Brackbill *et al*. [10] was used to model the surface tension. With CSF model, the addition of surface tension to the VOF model calculation results in an additional source term in the momentum equation (3).

$$\frac{\partial}{\partial t}(\rho u_j)+\frac{\partial}{\partial x_i}(\rho u_i u_j)=-\frac{\partial P}{\partial x_j}+\frac{\partial}{\partial x_i}\mu\left(\frac{\partial u_i}{\partial x_j}+\frac{\partial u_j}{\partial x_i}\right)+\rho g_j+F_j \tag{3}$$

where, P, g and F indicate, respectively, the pressure, the gravitational acceleration and the external force per unit volume, u_i is the i component of the fluid velocity u, x_j is the j spatial coordinate, μ is the dynamic viscosity.

For a two-phase flow system, if the phases are represented by the subscripts 1 and 2 and the volume fraction of the phase 2 is known, the ρ and μ in each cell are given by the following

equation:

$$\rho = \alpha_2\rho_2 + (1-\alpha_2)\rho_1, \mu = \alpha_2\mu_2 + (1-\alpha_2)\mu_1, \tag{4}$$

The interface between the two phases can be traced by solving the continuity equation for the volume fraction function for the secondary phase:

$$\frac{\partial \alpha_q}{\partial t} + \frac{u_i \partial(\alpha_q)}{\partial x_i} = 0 \tag{5}$$

Where u_i and x_i denote, respectively, the velocity component and the co-ordinate in the direction i (i = 1, 2 or 3), t, being the time; and through the resolution of the momentum equation shared by the two considered fluids.

The volume fraction equation for the primary phase in equation (5) will be obtained from the following equation:

$$\sum_{q=1}^{n} \alpha_q = 1 \tag{6}$$

No boundary condition on interface slip is specified in the VOF model, therefore the gas and liquid phases share a common velocity field, and the interface velocity is not directly calculated but, rather determined via interpolation of neighbouring velocities.

Solving these sets of equations has been done using a software package Star-CCM+. For the calculation of fluxes at control volume faces required by the VOF model, a second order discretization scheme was used, as recommended by the code documentation.

3.3.1 Surface tension and wall adhesion

The VOF method incorporated the effect of surface tension along the interface between the phases. In the present work, the contact angle between the phases and the wall was specified in the model and the surface tension coefficient was taken as a constant. It is worthy of mention again that the surface tension model uses the continuum surface force (CSF) model Brackbill *et al*. [10]. In this model, the addition of surface tension to the VOF calculation results in a source term in the momentum equation where the pressure drop across the surface can be obtained from surface tension coefficient σ and the surface curvature which is measured by two radii in the orthogonal directions R_1 and R_2 using Young-Laplace equation (7) as follows,

$$p_2 - p_1 = \sigma\left(\frac{1}{R_1} + \frac{1}{R_2}\right) \tag{7}$$

Where, p_1 and p_2 are the pressures in the two fluids on either sides of the interface [37].

The surface tension can be written in terms of the pressure jump across the surface. The force at the surface can be expressed as a volume force using the divergence theorem. It is this volume force that is the source term which is added to the momentum equation (3). It has the form of equation (8):

$$F_{vol} = \sum_{ij, i<j} \sigma_{ij} \frac{\alpha_i \rho_i k_j \nabla\alpha_j + \alpha_j \rho_j k_i \nabla\alpha_i}{\frac{1}{2}\left(\rho_i + \rho_j\right)} \tag{8}$$

Equation (8) allows for a smooth superposition of forces near cells where more than two phases are present [37]. Since this work is concerned with two-phase flow, only two phases will be present in a cell, so that $k_i = -k_j$ and $\nabla\alpha_i = -\nabla\alpha_j$, equation (8) then simplifies to equation (9)

$$F_{vol} = \sigma_{ij} \frac{\rho k_i \nabla \alpha_i}{\frac{1}{2}\left(\rho_1 + \rho_2\right)} \tag{9}$$

Where ρ is the volume-averaged density computed using equation (4)

3.4 Turbulence model

For the flow condition of this work, turbulence is evident from different points of view, such as the Reynolds Number and mixing process at the tail of the Taylor bubble, even in low flow rates. In addition, the bend has been reported to be a major source of turbulence [1]. Therefore, turbulence must be considered in the numerical simulation. The accuracy of CFD solutions for turbulent flows can be affected by turbulence modelling, especially because of the complex features of the flow. According to Versteeg and Malalasekera [42], it has been recognized by the CFD community that, the choice of turbulence models used to represent the effect of turbulence in the time-averaged mean-flow equations represents one of the principal sources of uncertainty of CFD predictions. In order to simulate turbulence, the standard k-ε model, [28], which requires that the flow is fully turbulent, was used for several reasons; the model is computationally-efficient, is implemented in many commercial codes, the pipe geometry is not complicated and it has demonstrated capability to simulate properly many industrial processes, including multiphase flow. The model is described by the following elliptic equations required as closure for the RANS equations:

$$\rho u_j \frac{\partial k}{\partial x_j} = \frac{\partial}{\partial x_j}\left(\frac{\mu_t}{\sigma_k}\frac{\partial k}{\partial x_j}\right) + \mu_t \frac{\partial u_j}{\partial x_i}\left(\frac{\partial u_i}{\partial x_j} + \frac{\partial u_j}{\partial x_i}\right) - \rho\varepsilon \tag{10}$$

$$\rho u_j \frac{\partial \varepsilon}{\partial x_j} = \frac{\partial}{\partial x_j}\left(\frac{\mu_t}{\sigma_\varepsilon}\frac{\partial \varepsilon}{\partial x_j}\right) + C_1 \mu_t \frac{\varepsilon}{k}\frac{\partial u_j}{\partial x_i}\left(\frac{\partial u_i}{\partial x_j} + \frac{\partial u_j}{\partial x_i}\right) - C_2 \frac{\varepsilon}{k}\rho\varepsilon \tag{11}$$

In the above equations, k is the turbulent kinetic energy; ε is the dissipation rate of k. σ_k, σ_ε, C_1 and C_2 are constants whose values are 1.0, 1.3, 1.44 and 1.92 respectively, u_i is the i component of the fluid velocity u, x_j is the j spatial coordinate. The fluid viscosity must be corrected for turbulence in the Navier-Stokes equations employing an effective viscosity $\mu_{eff} = \mu + \mu_t$ where μ is the dynamic viscosity and μ_t is the turbulent viscosity.

3.5 Boundary conditions

Once the mesh was generated, the boundaries of the computational domain were specified. Boundary types are specified in order to define the physical and operational characteristics of the model at the model boundaries. It is worth mentioning that the imposition of boundary conditions depends on the physics of the problem and have to be treated with care. Hence, the boundary conditions were chosen based on the experimental setup.

The summary of the boundary specifications is as follows:

Inlet …… (Velocity inlet) Dirichlet Boundary condition $\hat{n}.\bar{v} = U_o$

Outlet ……..... (Pressure outlet) Neumann Boundary condition $P = P_o$

Wall……Wall $\hat{n}.\bar{v} = \hat{t}.\bar{v} = 0$

Where $\hat{n}.\bar{v}$ = no penetration and $\hat{t}.\bar{v}$ no slip

All solid boundary walls were assumed to possess a non slip boundary condition, $v = 0$. At the flow inlet at the base of the riser, a velocity-inlet boundary type is used in which the mixture superficial velocity and the liquid void fraction are specified. The velocity profile is assumed to be uniform. This approach according to Hernandez-Perez [23] requires no additional experimental knowledge about the inlet flow pattern in order to setup the numerical simulation. This is also similar to the way experimental work has been carried out (see [1] for details about the mixing section design). The volume fraction and density of each phase were both prescribed at the inlet. The inlet values for turbulent kinetic energy, k, and its dissipation rate, ε, are estimated with the

following equations proposed by [28]:

$$k_{in} = \frac{3}{2} I^2 U_{in}^2 \tag{12}$$

$$\varepsilon_{in} = 2k_{in}^{3/2} / d \tag{13}$$

$$I = \frac{0.16}{\mathrm{Re}^{1/8}} \tag{14}$$

Where d is the pipe diameter, and I the turbulence intensity for fully developed pipe

The values of the turbulent intensity, turbulent kinetic energy and turbulent dissipation rate are given in Table 3

Table 3: Boundary conditions

Inlet condition	Value
Turbulent intensity	0.06
Turbulent kinetic energy (J/kg)	0.0043
Turbulent dissipation rate (J/kgs)	0.01

The walls of the pipe are assumed to be rigid and impermeable, in which the wall roughness was set as a smooth wall. A no-slip condition is applied to the velocity where there is contact at solid walls at any instant. Close to the wall, the standard wall function approach [28] was employed to predict accurately the flow close to the walls. At the flow outlet at the top of the horizontal pipe (downstream of the vertical 90° bend), the remaining variables are transported out of the computational domain with zero average static pressure so that the mass flow balance is satisfied. The operating conditions were specified as being standard atmospheric pressure (101.3 *kPa*) and temperature 20°C. Gravity effects are accounted for and the acceleration due to gravity to be -9.81 m/s^2 on the vertical.

3.6 Initial conditions

At time t = 0 second all velocity components are set to 0 m/s ($t = t_o\ \hat{n}.\bar{v} = \mathrm{V}_o$). For the liquid volume fraction, the specified initial condition depended on the case under study; in this work, the initial condition was the pipe full of air or silicone oil. These initial conditions ease the convergence process. In addition, an initial guess for the turbulent kinetic energy and the dissipation rate were applied in the simulation.

3.7 Discretization and Solution algorithm

The system of governing partial differential equations have been numerically solved via discretization of the equations using a Finite Volume Method (FVM) with an algebraic segregated solver and co-located grid arrangement, as implemented in [37]. In this grid arrangement, pressure and velocity are both stored at cell centres. The second-order upwind differencing scheme is used for solving the momentum equation to minimize numerical diffusion and the first order explicit time marching scheme is used for solving the unsteady formulation. The interface between gas and liquid are reconstructed using piecewise linear interface calculation (PLIC) proposed by Youngs [45]. Since Star-CCM+ uses a segregated solver for VOF, the continuity and momentum equations need to be linked. To achieve the linkage, various techniques are reported in the literature. The Semi-Implicit Method for Pressure-Linked Equations (SIMPLE) algorithm, (Patankar and Spalding [35]), is applied to control the overall solution because of its good performance to find a fast

converged solution. In addition, the iterative solver was speeded up tremendously by using an Algebraic Multigrid (AMG) technique to yield a better convergence rate. When large body forces exist in gas–liquid flows, the body force and pressure gradient terms in the momentum equation tends to be almost in equilibrium, with the contributions of convective and viscous terms small comparatively. Many methods are used to improve the accuracy and convergence of the VOF solution. Segregated algorithms converge poorly unless partial equilibrium of pressure gradient and body forces is taken into account, and an optional implicit body force treatment that can account for this effect, making the solution more robust.

A time marching scheme has been used due to the nature of the problem, which is time dependent. For the time dependent solution scheme, the main controlling factor is the time step. This is set to give a small number of time steps as possible whilst maintaining a smoothly converging solution. For this reason, the time step size was set as 10^{-4} s, maximal iterations per time step was 100, and the total simulation time was 23 s, which is enough for a Taylor bubble and liquid slugs to move from the riser to the flowline via the 90º bend.

Again, for this iteration process to converge, it may be necessary to control the change of the variables from one iteration to the next. This is achieved with under relaxation factors. Under relaxation factors of 0.3, 0.7 and 0.8 respectively were applied on pressure, momentum and turbulence kinetic energy parameters, as recommended by [37].

4. RESULTS AND DISCUSSION

The comparison between the results obtained from the CFD simulation and experiment involving both before and after the vertical 90º bend will be based on time series of void fraction and probability density function (PDF) of void fraction. To achieve this, two experimental campaigns were conducted using the ECT and WMS. The first experimental campaign involved the use of ECT and WMS placed at: (1) before the bend using both instruments at different sections of the pipe and (2) involved the use of the WMS placed some distance after the bend. This will be carried out at same liquid and gas superficial velocities of 0.05 and 0.34 m/s, respectively. The model fluid is air–silicone oil. The number of cells used for the CFD calculation is 500,000 cells. This is based on the grid convergence studies carried out by [1] and [39].

4.1 Comparison between the Computational fluid dynamics (CFD) and experiment before the vertical 90º bend (first case):

Here, we compare the results of CFD and experiment before the vertical 90º bend based on the time series of void fraction and probability density function (PDF) of void fraction. This is presented on Table 4. The PDF is the probability that the void fraction values lie within a certain range ($\varepsilon \pm \delta\varepsilon$). The PDF was determined by grouping void fraction values in data bins of width 0.01. This results in 100 bins centered on 0.005, 0.015…0.995, and then the number of data points in each bin is divided by the total number of data points in the time series. The PDFs indicate the dominant void fractions which are observed for each flow condition. As described before, the experimental part involved the use of ECT and WMS placed upstream of the bend. The ECT is made up of 2 planes; planes 1 and 2 separated by a distance of 89 mm. ECT-plane 1 is located at 4.4 m downstream of the two-phase mixing section. The WMS on the other hand, is located at a distance of 4.92 m away from the two-phase mixing section. The CFD simulation, similar to the experimental arrangements, had three measurement sections, ECT-plane 1, ECT-plane 2 and WMS corresponding to the same measurement location of the experiment. This provides the opportunity of comparing like with like in terms of measurement locations.

Table 4 shows that there is a reasonably good agreement between CFD and experiments based on the time series of void fraction and PDF of void fraction. The table shows that at liquid and gas superficial velocity of 0.05 m/s and 0.34 m/s, respectively before the bend, using both the ECT (ECT-plane 1 and ECT-plane 2) and WMS, the experiment and CFD predict same flow pattern, slug flow. This is according to the time series of void fraction and PDF of void fraction. Though, the shape of the PDF of void fraction for the CFD and experiment are similar. The plot for the experiment is smoother than for the CFD. This is to be expected considering the fact that the experiment was carried within a duration of 60 seconds whilst the CFD, 23 seconds.

It is interesting to observe that at steady state, the time series of void fraction for the experiment, involving the ECT-plane 1, ECT-plane 2 and WMS are very similar to those of the CFD. For the

ECT-plane 1, the height of the peak of the void fraction for the experiment and CFD are 0.79 and 0.795, respectively. The percentage error is 0.6. Moving to the ECT-plane 2 shows the height of the peak of the void fraction for both the experiment and CFD has increased to 0.81. At the location of the WMS, the height of the peak of the void fraction remained same as that of ECT-plane 2.

On the other hand, the PDF of fraction for the experiment involving ECT-plane 1, show a double peak: one at a lower void fraction representing liquid slug and the other at a higher void fraction, Taylor bubble. The height of the peak of the PDF of void fraction though is 0.058. The CFD scenario also shows a double peak, but with the height of the peak equal to 0.04. The percentage error is 31. For the ECT-plane 2, the heights of the PDF of void fraction for both the experiment and CFD have dropped to 0.058 and 0.37, respectively. Though, both the experiment and CFD both predict same flow pattern, slug flow. For the WMS, both the experiment and CFD also predict same flow pattern, slug flow. The height of the PDF of void fraction for both the experiment and CFD are 0.42 and 0.32, respectively. This corresponds to an error of 24 %.

Table 4: Flow pattern comparison between experiment and CFD before the vertical 90° bend (Steady-state)

	EXPERIMENT		CFD	
Instrument @ location	Time series of void fraction	PDF of void fraction	Time series of void fraction	PDF of void fraction
ECT-Plane 1 @ 4.4 m	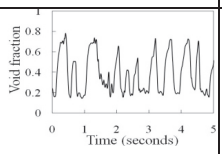	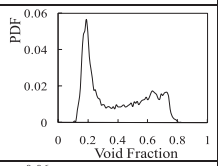	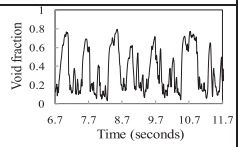	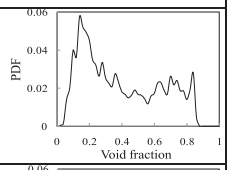
ECT-Plane 2 @ 4.489 m	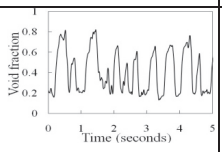	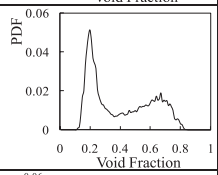	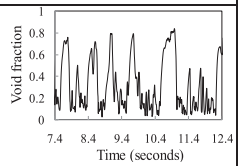	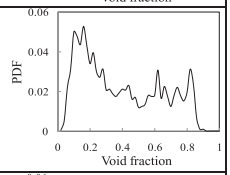
WMS @ 4.92 m	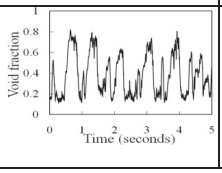	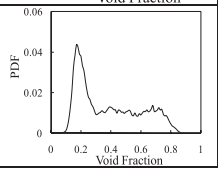	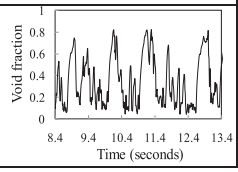	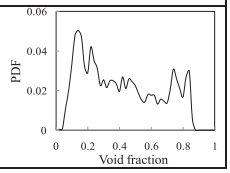

4.2 Comparison between the Computational fluid dynamics (CFD) and experiment after the vertical 90º bend (second case):

The flow pattern approaching the vertical 90º bend as shown in Figure 3 is slug flow. After the bend, the two-phase flow distribution is completely different when compared to the flow upstream of it. At the bend in a vertical plane, one would expect separation tendencies to increase with density difference and axial velocity to decrease with bend radius. According to Carver and Salcudean [13], separation force depends on the vectorial sum of the gravitational and centrifugal forces, which varies throughout the bend. Therefore, according to [1], the variation of the orientation will greatly affect the phase distribution and can lead to separation. Again, [13] claimed that when the phase separation is observed, one can distinguish three sections namely, continuous liquid, continuous gas and dispersed phase.

It can be observed from Figure 3 that both the Taylor bubble and liquid slug move to the outside of the bend owing to the action of centrifugal force and on the other hand, the gravity force drains the liquid in the liquid slug and liquid film in the annulus to the inside of the bend. This interesting observation is depicted in Figures 3-7. This behaviour is similar to the observations reported by Abdulkadir *et al.* [3] who carried out experimental work on a vertical and horizontal 90º bends using air and silicone as the model fluids.

The time series of void fraction and PDF of void fraction obtained downstream of the bend shows that the prevailing flow pattern is stratified wavy as shown in Table 5. This is confirmed by the cross-sectional contour plot of void fraction at 45 and 90°, respectively, shown in Figure 5a - b. This is also reinforced by the output of the WMS illustrated in Figure 5: showing the position of the gas and liquid downstream of the bend. The time series of void fraction presented in Table 5 for both the experiment and CFD show maximum peaks of 0.82 and 0.81, respectively. The percentage error is 1. On the other hand, the PDF of void fraction show highest peaks of 0.08 and 0.09 for experiment and CFD, respectively. For the experiment, the void fraction corresponding to the maximum peak of void fraction is 0.8 but with a broadening tail down to 0.2 while for the CFD, the void fraction is 0.75 with a tail down to 0.25.

Table 5: Flow pattern comparison between experiment and CFD after the vertical 90° bend

	EXPERIMENT		CFD	
Instrument @ location	Time series of void fraction	PDF of void fraction	Time series of void fraction	PDF of void fraction
WMS @ 0.21 m	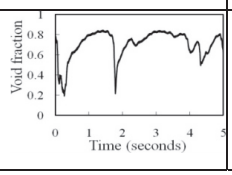	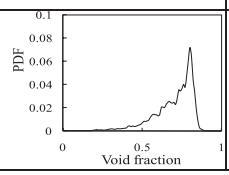	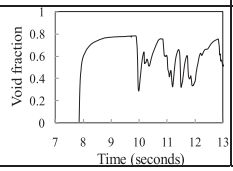	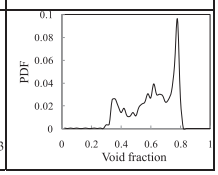

The contour plot of void fraction presented in Figure 3 show a detailed appearance of a train of Taylor bubbles separated by liquid slugs. It is interesting to observe from the figure, the comparison between the outputs of the experiment and the CFD and also the confirmation by the high speed video image.

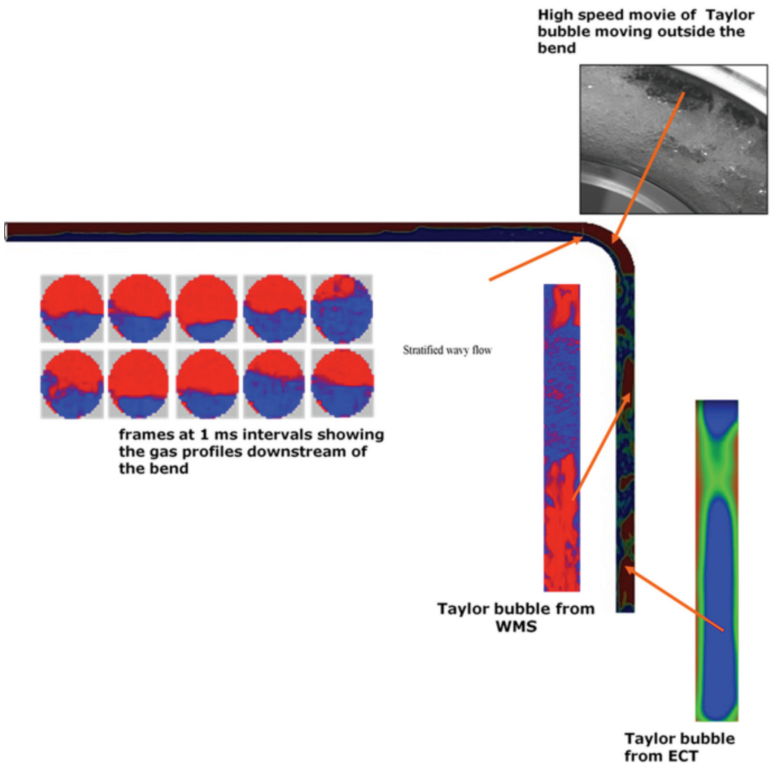

Figure 3: Contour plot of void fraction

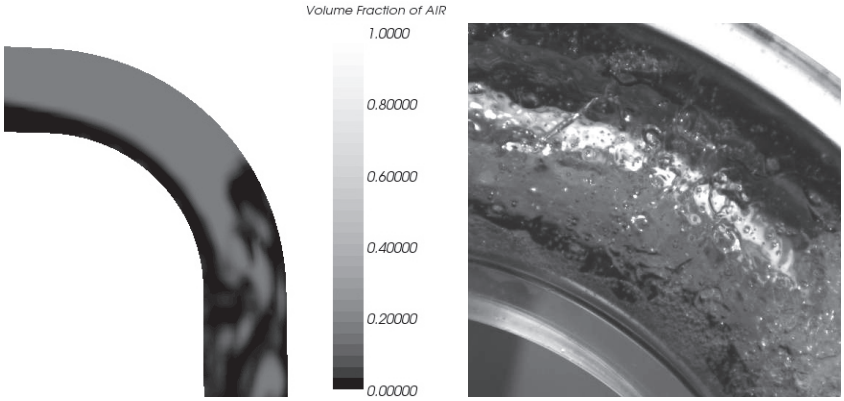

Figure 4 Comparison between the (a) CFD contour plot of void fraction and (b) video image of slug flow passing through a vertical 90º bend at liquid and gas superficial velocities of 0.05 and 0.34 m/s, respectively

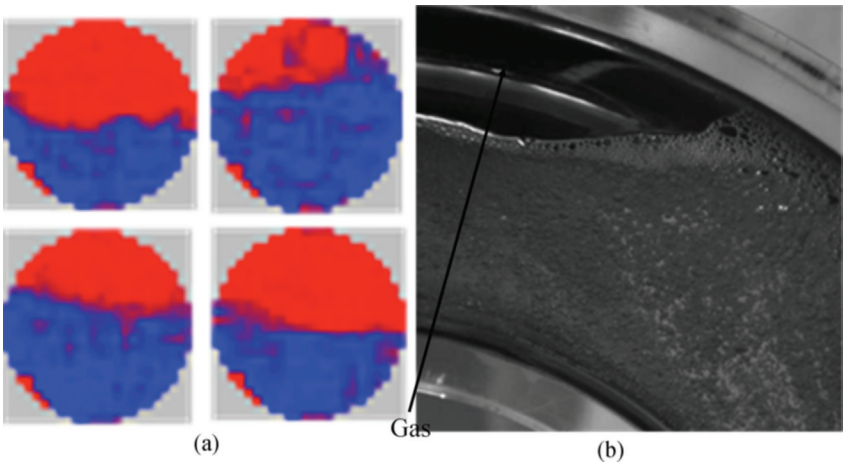

Figure 5 (a) Sequence of frames at 1 ms from WMS and (b) Video image showing the location of the gas, top and liquid, bottom of the pipe at liquid and gas superficial velocities of 0.05 and 0.34 m/s, respectively. Red colpur represents gas, blue liquid

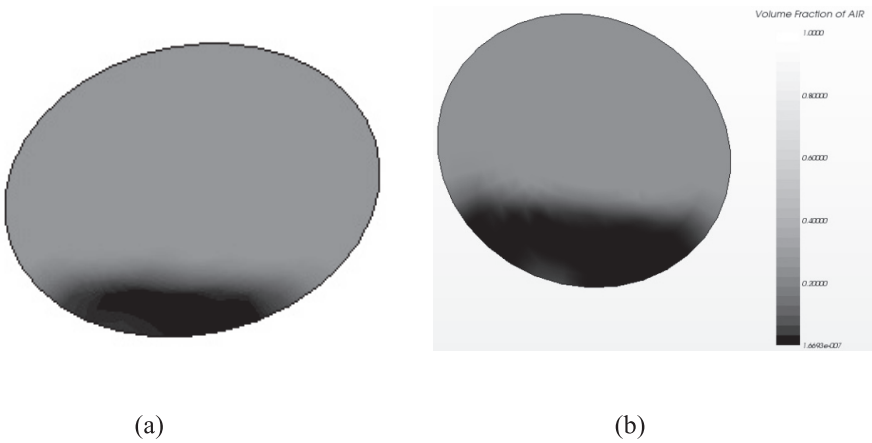

Figure 6: cross-sectional contour plot of void fraction located at: (a) 45º and (b) 90º into the bend

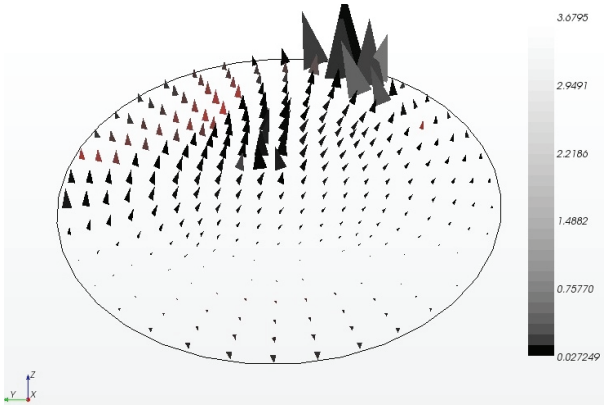

Figure 7: cross-sectional contour plot of velocity located at 45º into the bend

4.3 Flow development downstream of the bend

The comparison between the results obtained from experiments and CFD downstream of the bend was carried out at 0.21 m using the WMS. However, the most distant section (length of the horizontal pipe) from the bend is 2 m (26 pipe diameters). In the literature some researchers, including [23], have recommended a development distance of about 40 pipe diameters for a horizontal pipe. In addition, the flow pattern frequently depends upon the observation position along the test section. It is very important therefore to know at what location downstream of the bend the flow can be considered fully developed. This knowledge according to [1] will inform flow assurance experts where to place partial phase separators or dividing junctions in order to collect the separated phases. To circumvent this challenge, a flow development study is carried out using CFD. This involved selecting seven measurement locations downstream of the bend as shown in Table 6.

Table 6: Interrogating flow development downstream of the bend

Location after the bend (m)	Time series of void fraction	PDF of void fraction
0.21 (3 pipe diameters)	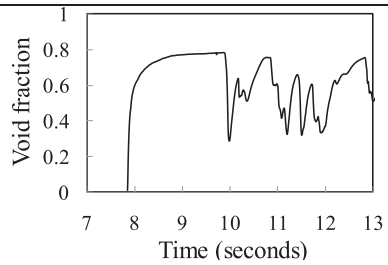	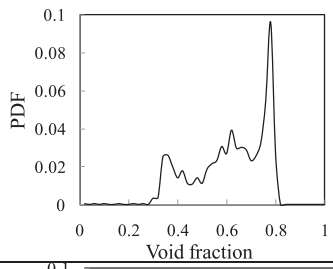
0.5 (7 pipe diameters)	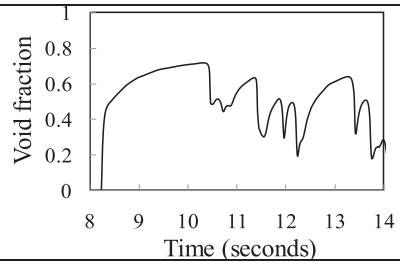	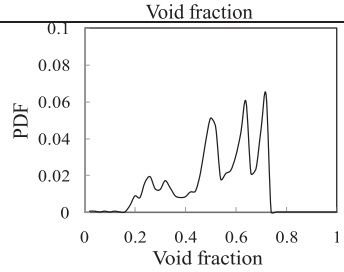

Continued

0.75 (11 pipe diameters)	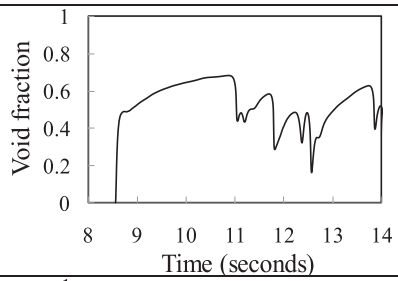	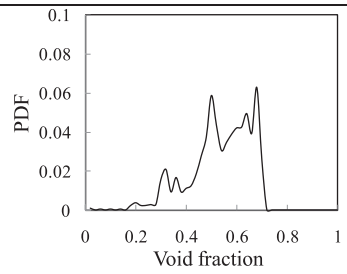
1.0 (15 pipe diameters)	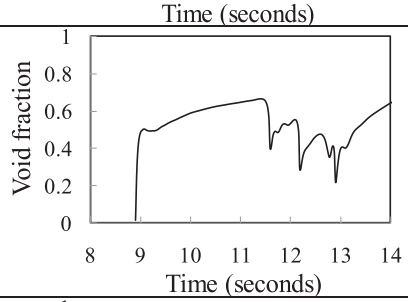	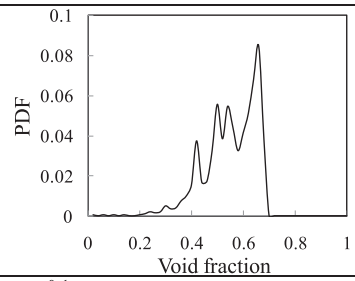
1.25 (19 pipe diameters)	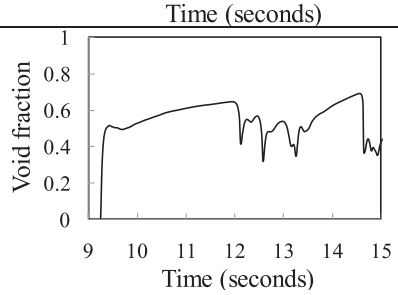	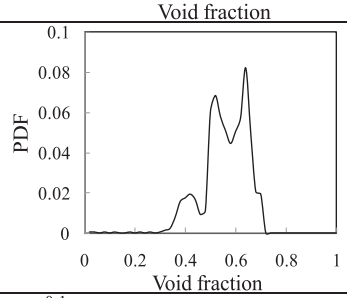
1.5 (22 pipe diameters)	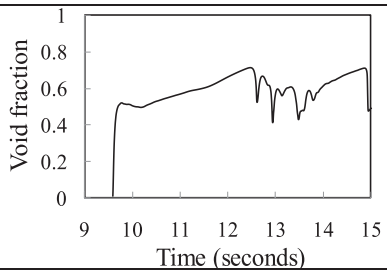	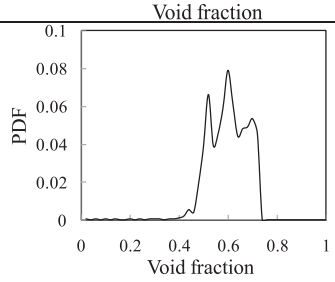

Time series of void fraction, and PDF of void fraction obtained from the CFD simulation are used to assess the change in flow characteristics with distance downstream of the bend. The advantage of the CFD simulation compared to the experiment is the possibility to record the time series of void fraction at many measurement sections along the pipe. The simulations were performed within a flow domain of 6 m long vertical pipe joined to a 2 m horizontal pipe via a 0.154 m radius of curvature vertical 90º bend. Table 6 shows simulation results of time varying void fraction and PDF of void fraction derived from the seven measurement locations at liquid and gas superficial velocities of 0.05 and 0.34 m/s, respectively.

It can be observed from the time series of void fraction shown in Table 6 that the length of the trailing bubbles increases with an increase in the axial distance. This can be explained by the occurrence of bubble coalescence. The PDF of the time series of void fraction at 0.21 m, just downstream of the bend, shows a characteristic signature of stratified wavy flow. It also shows that the results obtained from 0.21 m are initially affected by the bend. This is further reinforced by the PDF of void fraction. The flow patterns begin to change to stratified flow at a distance of about 1.25 m (19 pipe diameters) from the bend. At a distance of 1.25 m from the bend, both the time series and PDF of void fraction begin to take the shape of stratified flow. Though, it becomes more apparent at 1.5 m from the bend. It could be concluded that the flow becomes developed at around 20 pipe diameters.

5. CONCLUSIONS

In this work, detailed simulation of slug flow in a vertical 90º bend has been carried out using the VOF method available in commercial code Star-CD and Star-CCM+. The simulations and experiments were performed within a flow domain of 6 m long vertical pipe with a 0.067 m internal diameter connected to a 2 m long flowline via a vertical 90º bend (bend radius of 0.1544 m) charged with an air and silicone oil mixture as the working fluid. A comparison of the results obtained from CFD simulation and experiments both before and after the vertical 90º bend based on time series of void fraction, PDF of void fraction and cross-sectional contour plot of void fraction were successfully carried out and the following conclusions can be drawn:

1. The CFD simulation is able to predict both the flow pattern before and after the bend. These results were confirmed by the high-speed videos taken around the bend.
2. A reasonably good agreement was obtained, and the CFD simulation can be used to locate the position of the gas phase in the bend with confidence. However, further parametric CFD studies might be required to close the gap between CFD simulations and the experimental results.
3. The flow pattern downstream of the bend is developed at 1.5 m (22 pipe diameters) and that the partial phase separator or dividing junction should be designated at this location.

NOMENCLATURE

In this section a list of symbols not defined in the main text is given

A	Area [m^2]
F	Frequency [Hz]
g	Gravitational acceleration [m/s^2]
k	Kinetic energy of turbulence [m^2/s^2]
n	number of phases [-]
t	Time [s]
u	Velocity [m/s]
μ	Dynamic viscosity [kg/ms]
ρ	Material density [kg/m^3]
σ	Surface tension [N/m]
i,j	Space directions
q	Phase index

ACKNOWLEDGEMENTS

M. Abdulkadir would like to express sincere appreciation to the Nigerian government through the Petroleum Technology Development Fund (PTDF) for providing the funding for his doctoral studies.

This work has been undertaken within the Joint Project on Transient Multiphase Flows and Flow Assurance. The Authors wish to acknowledge the contributions made to this project by the UK Engineering and Physical Sciences Research Council (EPSRC) and the following: - Advantica; BP Exploration; CD-adapco; Chevron; ConocoPhillips; ENI; ExxonMobil; FEESA; IFP; Institutt for Energiteknikk; Norsk Hydro; PDVSA (INTERVEP); Petrobras; PETRONAS; Scandpower PT; Shell; SINTEF; Statoil and TOTAL. The Authors wish to express their sincere gratitude for this support.

REFERENCES

[1] Abdulkadir, M., 2011. Experimental and computational fluid dynamics (CFD) studies of gas-liquid flow in bends. PhD Thesis, University of Nottingham, United Kingdom.

[2] Abdulkadir, M., Hernandez-Perez, V., Sharaf, S., Lowndes, I. S., and Azzopardi, B. J., 2010. Experimental investigation of phase distributions of an air–silicone oil flow in a vertical pipe. *World Acad. of Sci., Eng' g and Tech.* (WASET), 61, pp.52-59

[3] Abdulkadir, M., Zhao, D., Sharaf, S., Abdulkareem, L., Lowndes, I.S., and Azzopardi, B. J., 2011. Interrogating the effect of 90º bends on air–silicone oil flows using advanced instrumentation. Chem. *Eng Sci*., 66, pp. 2453-2467.

[4] Abdulkadir, M., Hernandez-Perez, V., Lowndes, I.S., and Azzopardi, B. J., and Dzomeku, S. 2014. Experimental study of hydrodynamic behaviour of slug flow in a vertical riser. Chem. Eng. Sci. 106, pp.60-75

[5] Azzopardi, B. J., 1997. Drops in annular two-phase flow. *Int. J. Multiphase Flow* 23, pp. S1-S53.

[6] Azzopardi, B. J., Abdulkareem, L.A., Sharaf, S., Abdulkadir, M., Hernandez-Perez, V., and Ijioma, A., 2010. Using tomography to interrogate gas–liquid flow. In: 28th UIT Heat Transfer Congress, *Brescia*, Italy, pp. 21-23 June.

[7] Akagawa, K., and Sakaguchi, T., 1966. Fluctuation of void fraction in gas–liquid two-phase flow. *Bulletin JSME*, 26, pp. 627-638

[8] Bagci, S., 2003. An investigation of two-phase slug flow in inclined pipelines. Ener. *Sources*, 19, pp. 829-838

[9] Barnea, D., and Brauner, N., 1993. A model for slug length distribution in gas–liquid slug flow. *Int. J. Multiphase Flow* 19, pp. 829-838

[10] Brackbill, J.U., Kothe, D.B., and Zemach, C. 1992. A continuum method for modelling surface tension. *J. Comput. Phys.* 100, pp. 335-354.

[11] Brauner, N., and Ullmann, A., 2004. Modelling of gas entrainment from Taylor bubbles, Part A: Slug flow. *Int. J. Multiphase Flow* 30, pp. 239 - 272

[12] Brown, R. A. S., 1965. The mechanics of large gas bubbles in tubes: I. Bubble velocities in stagnant liquids. Can. J. Chem. *Eng.* 43, pp. 217-223

[13] Carver, M.B., and Salcudean, M., 1986. Three-dimensional numerical modelling of phase distribution of two-fluid flow in elbows and return bends. Num. *Heat Transfer* 10, pp. 229-251

[14] Clarke, A., and Issa, R. I., 1997. A numerical model of slug flow in vertical tubes. Comput. *Fluids* 26, 4, pp. 395 - 415.

[15] Collins, R., De Moraes, F. F., Davidson, J. F., and Harrison, D., 1978. The motion of a large gas bubble rising through liquid flowing in a tube. *J. Fluid Mech.* 89, pp. 497-514.

[16] da Silva, M.J., Thiele, S., Abdulkareem, L., Azzopardi, B.J., and Hampel, U., 2010. High-resolution gas-oil two-phase flow visualization with a capacitance wire-mesh sensor. *Flow Meas. Instrum.* 21, pp. 191-197.

[17] DeJesus, J.D., Ahmad, W., and Kawaji, M., 1995. Experimental study of flow structure in vertical slug flow. *Adv. in Multiphase Flow* 31, pp.105-118

[18] Dumitrescu, D. T. 1943. Stromung an einer luftblase in senkrechten rohr Z angrew *Math Mech*, 23, pp. 139-149

[19] Fabre, J., and Line, A., 1992. Modelling of two-phase slug flow. Annu. Rev. *Fluid Mech.* 24, pp. 21-46

[20] Fernandes, R. C., Semiat, R., and Dukler, A.E., 1983. Hydrodynamics model for gas - liquid slug flow in vertical tubes. *AIChE J.* 29, pp. 981-989

[21] Geraci, G., Azzopardi, B. J., and Van Maanen, H. R. E., 2007a. Inclination effects on circumferential film distribution in annular gas/liquid flows. *AIChE J.* 53, 5, pp. 1144 -1150.

[22] Geraci, G., Azzopardi, B. J., and Van Maanen, H .R .E. 2007b. Effects of inclination on circumferential film thickness variation in annular gas/liquid flows. *Chem. Eng. Sci.* 62, 11, pp. 3032 - 3042.

[23] Hernandez-Perez, V., 2008. Gas–liquid two-phase flow in inclined pipes. PhD thesis, University of Nottingham.

[24] Hernandez-Perez, V., Abdulkadir, M., and Azzopardi, B. J., 2011. Grid generation issues in the CFD modelling of two-phase flow in a pipe. *The J. of Computational Multiphase Flow* 3, pp. 13 - 26

[25] Hammer, E. A., 1983. Three–component flow measurement in oil/gas/water mixtures using capacitance transducers. PhD thesis, University of Manchester

[26] Hirt, C. W., and Nichols, B. D., 1981. Volume of fluid (VOF) method for the dynamics of free boundaries. *J. Comput. Phys.* 39, pp. 201.

[27] Huang, S. M., 1995. Impedance sensors-dielectric systems. In R. A. Williams, and M. S. Beck (Eds.). Process Tomography, Cornwall: Butterworth-Heinemann Ltd.

[28] Launder, B., and Spalding, D., 1974. The numerical computation of turbulent flows. Comput. Meth. Appl. *Mech. Eng.* 3, pp. 269-289.

[29] Lo, S., and Zhang, D., 2009. Modelling of break-up and coalescence in bubbly two-phase flows. The *J. of Computational Multiphase Flow* 1, pp. 23 -38

[30] Mao, Z. S., and Dukler, A.E., 1985. Brief communication: Rise velocity of a Taylor bubble in a train of such bubbles in a flowing liquid. *Chem. Eng. Sci.* 40, pp.2158-2160

[31] Mao, Z. S., and Dukler, A. E., 1991. The motion of Taylor bubbles in vertical tubes. II. Experimental data and simulations for laminar and turbulent flow. *Chem. Eng. Sci.* 46, pp.2055-2064.

[32] Moissis, R., and Griffith, P., 1962. Entrance effects in two-phase slug flow. *ASME J. of Heat Transfer*, pp. 366-370

[33] Muzaferija, S., and Peric, M., 1999. Computation of free surface flows using interface-tracking and interface-

capturing methods. Chap.2 in O. Mahrenholtz and M. Markiewicz (eds.), Nonlinear Water Wave Interaction, Comp. Mechanics Publication, WIT Press, Southampton

[34] Nicklin, D. J., Wilkes, J. O., and Davidson, J. F., 1962. Two-phase flow in vertical tubes. *Transaction of Inst. of Chemical Engineers* 40, pp. 61-68

[35] Patankar, S.V., Spalding, D.B., 1972. A calculation procedure for heat, mass and momentum transfer in three dimensional parabolic flows. *Int. J. of Heat and Mass Transfer* 15, pp. 1787.

[36] Pinto, A. M. F. R., and Campos, J. B. L. M., 1996. Coalescence of two gas slugs rising in a vertical column of liquid. Chem. *Eng. Sci.* 51, pp. 45-54

[37] Star-CD Version 4.10 and Star-CCM+ Documentation, 2009. CD-adapco

[38] Taha, T., and Cui, Z.F., 2006. CFD modelling of slug flow in vertical tubes. Chem. *Eng. Sci.* 61, pp. 676-687

[39] Tkaczyk., P., 2011. CFD simulation of annular flows through bends. PhD thesis, University of Nottingham, United Kingdom.

[40] Ubbink, O., 1997. Numerical prediction of two fluid systems with sharp interfaces. PhD thesis, University of London

[41] van Houst, R., Barnea, D., Shemer, L., 2002. Translational velocities of elongated bubbles in continuous slug flow. *Int. J. Multiphase Flow* 28, pp. 1333-1350.

[42] Versteeg, H.K., Malalasekera, W., 2007. An Introduction to Computational Fluid Dynamics: the Finite Volume Method. 2nd ed. Pearson Educational Limited.

[43] Wallis, G. R., 1969. One-dimensional two-phase flow. McGraw-Hill, New York

[44] White, E. T., Beardmore, R. H., 1962. The velocity of rise of single cylindrical air bubbles through liquids contained in vertical tubes. Chem. *Eng. Sci.* 17, pp. 351-361.

[45] Youngs, D.L., 1982. Time-dependent multi material flow with large fluid distortion, in: K.W. Morton, M.J. Baines (Eds.). Num. M. for Fluid Dynamics, Academic Press, New York, pp. 273-285

[46] Zhu, K., Madhusudana Rao, S., Wang, C., Sundaresan, S., 2003. Electrical capacitance tomography measurements on vertical and inclined pneumatic conveying of granular solids. *Chem. Eng. Sci.* 58, pp. 4225-4245